The internal and external flow fields of a structured porous coated cylinder and implications on flow-induced noise

Arcondoulis, Elias J. G.; Ragni, Daniele; Rubio Carpio, Alejandro; Avallone, Francesco; Liu, Yu; Yang, Yannian; Li, Zhiyong

DOI
10.2514/6.2019-2648

Publication date
2019

Document Version
Final published version

Published in
25th AIAA/CEAS Aeroacoustics Conference

Aeroacoustics Conferences
20-23 May 2019, Delft, The Netherlands
25th AIAA/CEAS Aeroacoustics Conference

10.2514/6.2019-2648

The internal and external flow fields of a structured porous coated cylinder and implications on flow-induced noise

Elias J. G. Arcondoulis*
Southern University of Science and Technology, Shenzhen, Guangdong Province, 518055, China
Key Laboratory of Aerodynamic Noise Control, China Aerodynamics Research and Development Center, Mianyang, Sichuan Province, 62100, China

Daniele Ragni†, Alejandro Rubio Carpio‡ and Francesco Avallone§
Delft University of Technology, Delft 2629HS, The Netherlands

Yu Liu¶, Yannian Yang‖ and Zhiyong Li**
Southern University of Science and Technology, Shenzhen, Guangdong Province, 518055, China

Porous coated cylinders have been shown to reduce the vortex shedding tone and broadband noise of a bare cylinder placed in uniform flow within specific Reynolds number regimes. The processes by which the vortex shedding and thus tone suppression take place are still uncertain despite numerous numerical and experimental studies. It is understood that adding a porous medium to a bare cylinder will have an influence on the Reynolds number of cylinder, yet the increase of outer diameter alone and the influences of surface roughness are insufficient to explain the changes in the shedding tone magnitude and frequency that are observed by many. Investigating the internal flow field of a porous coated cylinder could lead to a deeper understanding of the flow processes that result in the tonal noise reduction. This has not been achieved to date, as commonly used materials such as metal foam and polyurethane possess randomized porous structures, which make investigating the internal flow field nearly impossible without affecting the structure itself. This paper presents a preliminary analysis of the internal and external flow fields of two structured porous coated cylinders. The cylinders were manufactured using solid transparent materials that possess direct lines of sight through the pores in the axial and spanwise directions. Such structured porous coated cylinders have been previously successful in reducing the typical vortex shedding tone. Tomographic and 2-D planar Particle Image Velocimetry (PIV) were used in a water-tunnel facility to visualize the internal and external flow fields. To date only the 2-D planar PIV results have been post-processed that reveal differences in the wake for the two different cylinder types such as recirculation of flow around the pores. Vorticity flow structures are observed to vary along the cylinder span in the same pattern as the porous structure and streamlines at the windward cylinder side reveal the entry of flow into the porous medium.

Nomenclature

d	=	bare cylinder diameter (mm)
D	=	porous coated cylinder outer diameter (mm)
f	=	acoustic frequency (Hz)
L	=	cylinder span (mm)
Re	=	Reynolds number
$Re_{\max}$	=	Maximum Reynolds number

*Postdoctoral Research Associate, Department of Mechanics and Aerospace Engineering, AIAA Member
†Assistant Professor, Department of Aerodynamics, Wind Energy, Flight Performance & Propulsion, AIAA Member
‡PhD Candidate, Department of Aerodynamics, Wind Energy, Flight Performance & Propulsion, Student AIAA Member
§Assistant Professor, Department of Aerodynamics, Wind Energy, Flight Performance & Propulsion, AIAA Member
¶Associate Professor, Department of Mechanics and Aerospace Engineering, Senior AIAA Member
‖Research Assistant Professor, Department of Mechanics and Aerospace Engineering, AIAA Member
**Postdoctoral Research Associate, Department of Mechanics and Aerospace Engineering, AIAA Member

St = Strouhal number
t = porous coating thickness (mm)
U = freestream flow velocity (m/s)
U_x = freestream flow velocity in the x-direction (m/s)
V_{SPCC} = porous coated cylinder volume (mm^3)
V_{SC} = equivalent solid cylinder volume (mm^3)
x, y, z = local coordinate directions
α = angle between the camera lens and the laser sheet (°)
θ = cylinder circumferential angle (°)
ϕ = porosity (%)
ω_y = vorticity about the y-axis (1/s)

I. Introduction

Passive flow control methods for cylinder bodies have become increasingly important for commercial and industrial applications such as parts of high speed train pantographs [1] and aircraft landing gear [2]. The flow-induced noise of a bare cylinder is composed of tonal and broadband noise [1] which can pose as a simplistic representation of typical noisy engineering components due to aeroacoustic interaction, such as a wind turbine pylon or a landing gear strut. The analysis of a single porous coated cylinder to approximate a high speed train pantograph component has also been shown to decrease the magnitude of tonal noise and decrease the tones frequency [3]. Geyer and Sarradj [4] observed that porous coating of a cylinder actually in some flow conditions strengthened the vortex shedding tone but decreased much of the broadband noise. Their more recent numerical simulations [5] agree with their experimental data. It should be noted that they used far less porous materials than the aforementioned literature. An interesting observation is that Sueki et al. [1] experimentally showed that the material type (i.e., comparing a Metal Foam Porous Coated Cylinder (MFPCC) to a Polyurethane Porous Coated Cylinder (PPCC)) had little or no impact on the measured noise reduction, thus showing that the porous material thickness, porosity and spacings of the pores were of greater importance in tonal and broadband noise reduction. Furthermore, suitable application of a porous coating to the cylinder leeward surface can lead to a significant reduction of drag as compared to a bare cylinder [6].

Arcondoulis et al. [7] calculated the average quantities pertaining to porous coated cylinders obtained from the literature, as of 2017; porous cover thickness to bare cylinder diameter ratio, $t/d \approx 0.22$, average minimum Reynolds number of $\approx 0.8 \times 10^5$ and an average maximum Reynolds number of $\approx 1.5 \times 10^5$. The majority of studies employ cylinders with a porous cover thickness to bare cylinder diameter ratio, t/d, of 0.1 to 0.5 and within $Re = 0.1 \times 10^5$ to 2×10^5. The important properties of porous media include the numbers of Pores Per Inch (PPI) and the porosity, ϕ, (as a percentage of the porous media volume with respect to a solid equivalent). The typical experimentally investigated PPI range, using metal foam and polyurethane for porous coated cylinders, is from 10 PPI to 30 PPI [1, 8–10], with significant vortex shedding tone reduction observed using 10 PPI materials [9, 10].

Several studies investigating the wake of a porous coated cylinder have been presented. Zradkovich [11] and Sueki et al. [8] applied a porous coating to the cylinder surface, revealing that a prolonged wake could minimize the lift and drag force fluctuations acting on the cylinder and that the wake of the porous coated cylinder is predominantly zero velocity. Aguiar et al. [9] observed that a more stabilized wake and a significant reduction in pressure drag coefficient occurs when treating a bare cylinder with a porous coating. Despite the growing understanding of the porous coated cylinder wake, few studies have been conducted to understand the internal flow field of a porous coated cylinder. This is important, as understanding the internal flow field leads to new porous coated cylinder designs that can be used to reduce drag, vortex induced vibration abd vortex shedding noise. Furthermore very few studies exist regarding the fundamental fluid mechanics properties of porous coated cylinders, such as the spanwise coherence length. Liu and Azarpeyvand [12] showed using delayed detached eddy simulations (DDES) at $Re = 1.66 \times 10^5$ that there was a negligible decrease of spanwise coherence of pressure fluctuations within six-diameters of the cylinder spanwise center, at circumferential angles of $\theta = 45°$ and 135°. They compared this to their results of a bare cylinder possessing a spanwise coherence length of approximately three-diameters, agreeing with experimentally obtained data [13, 14].

Arcondoulis et al. [7] designed a Structured Porous Coated Cylinder (SPCC), such that a clear line of sight is possible along the cylinder span and also from the outer porous coated cylinder surface into the internal solid cylinder. They showed that the tone suppression and frequency shift were very similar to PPCCs and MFPCCs with similar porosity and PPI. Figure 1 helps show the differences in porous structures typically used to treat cylinders for passive flow control. Due to the similar acoustic behavior of the SPCC relative to the randomized porous structures [7], it is

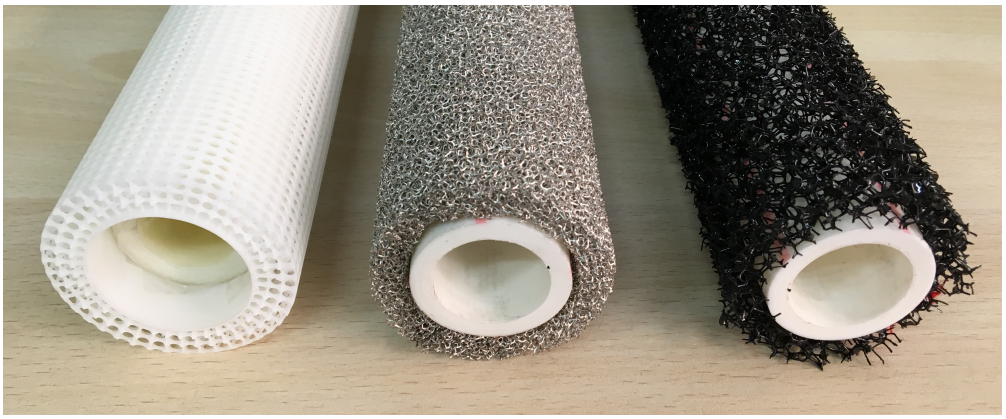

Fig. 1 Examples of porous coated cylinder types, illustrating the differences in porous coating structures that are used to treat cylinders as a form of passive noise control (from left to right: SPCC, MFPCC and PPCC).

hypothesized that the internal and external flow fields of these two different porous coated cylinder types should be very similar. The external flow field is relatively simple to compare for both cylinder types, by investigating time-averaged velocity profiles, linear instability analysis in the wake and turbulent kinetic energy levels. The internal flow field, however, is not simple to compare between the two cylinder types. The internal flow field of a structured porous coated cylinder could potentially be determined by carefully inserting a miniature hot-wire anemometry probe into the porous coated structure; however, near the internal solid surface reverse flow may occur and will thus be incapable of accurately measuring a boundary layer profile in these regions. The internal flow within the randomized porous medium is extremely difficult to measure without modifying the porous structure and thus affecting the flow behavior. It is believed that these difficulties have led to very few publications regarding the fundamental fluid mechanics properties of the internal flow field of a porous coated cylinder. Naito and Fukagata [15] presented numerically obtained boundary layer profiles within a porous layer, using a Brinkman-Forchheimer extended Darcy model approximation. They show on the bare cylinder surface that there exists a slip velocity and at some Reynolds numbers, reverse flow near the cylinder surface. Bruneau and Motazavi [16] developed a numerical method to simulate fluid flows within porous regions, which they used to show a significant decrease in vortex induced vibrations for several industrial and commercial applications. At low-Reynolds numbers Xue et al. [17] conducted a numerical investigation of 3-D flow through a single pore of open cell metal foam, revealing the internal flow field within a single pore yet it is difficult to determine the influence of the cylindrical geometry on the internal flow field as compared to a single, isolated pore. Despite these numerical simulations, there are no experimental data to verify these results.

In this paper, two similar SPCC designs are tested in a water tunnel using Tomographic and 2-D planar Particle Image Velocimetry (PIV). Both elliptical-shaped and square-shaped SPCC designs are investigated. By manufacturing the SPCCs using a transparent solid material, some of the internal flow field near the outer diameter is visualized and quantified. Unfortunately due to time limitations, only the 2-D planar PIV data are presented in this paper, yet the tomographic methodology used to obtain these data are discussed in detail and will be investigated as future work. The 2-D planar PIV tests reveal differences in the external flow fields of the two cylinders in the near wake. The investigation of the flow field on the windward side reveals that some of the flow indeed passes through the porous coating yet a typical solid cylinder streamline pattern is also observed around the cylinder, from circumferential angles of $\theta = 0°$ to 90°. The vorticity along the span on the windward side reveals an alternating negative-to-positive pattern that has a spacing matching the pore spacing, which likely indicates the penetration of the flow field into the cylinder along the cylinder mid-plane. Despite that the majority of the data has not been processed to date, this paper still reveals insight into some of the internal and external flow fields of structured porous coating cylinders. By adjusting the porosity, PPI and pore structure (i.e., elliptical and square-shaped pores), the near-wake of the SPCC shows some changes in the localized flow field that may impact the wake and therefore the overall vortex shedding mechanism. Post-processing the tomographic PIV data and interpreting the results is future work.

II. Cylinder Models

Two types of SPCCs ae used in this experimental investigation in order to investigate the effect of different structured porous coatings on the internal and external flow field. Furthermore, using two different SPCCs with different materials and manufacturing methods ensures that at least one of the models possesses sufficient transparency to conduct successful tomographic PIV tests within the outermost porous layer. Both cylinders possess the same porous coating thickness, t = 16 mm, and the same inner and outer diameter, d = 64 mm and D = 96 mm, respectively. Both cylinders also possess a span of L = 385 mm to accommodate the structural requirements of the support structures within the water tunnel testing facility. This section explains the selection of these parameters and the calculation of each porous coating's porosity, ϕ, and PPI.

A. Diameter and coating thickness selection

An iterative process of several interacting factors, such as the Reynolds number, outer diameter D and thickness-to-bare-diameter ratio t/d, and manufacturing limitations was conducted to design the SPCCs for a series of PIV tests in a water tunnel. The diameters of the SPCCs used for these experiments are larger than those used previously for aeroacoustic and PIV tests in air [7]. This is due to the differences in fluid medium (and required pore size to allow sufficient water-borne particles to enter the porous medium). In addition, the maximum allowable cylinder diameter is restricted by the potentially excessive blockage ratio of the cylinder in the water tunnel that possess a channel height of 300 mm. Also, the minimum allowable cylinder diameter is limited by the capability of manufacturing methods to create a structured porous structure on a smaller scale, where the structural members between the pores may be as thin as 1 mm. Therefore, the outer diameters are chosen to be D = 96 mm with an inner bare diameter of d = 64 mm and thus the ratio of the porous coating thickness to the bare cylinder diameter, t/d, is 0.25. This t/d ratio is consistent with the aeroacoustic investigation presented in Arcondoulis et al. [7] and within the typical t/d range of others [1, 3, 4, 8, 9, 12, 15, 18]. It is also important to ensure that the Reynolds number range is within the range of previously published data for comparative purposes. By using D = 96 mm and the maximum recommended flow speed in the water tunnel of $U_{\max}$ = 0.8 m/s, the maximum Reynolds number is calculated as $Re_{\max} = 7.3 \times 10^4$, assuming a water temperature of 18°C. This Reynolds number maximum is comparable with the published data of both porous coated cylinders [3, 4, 8, 10, 15] and bare cylinders [14, 19–21].

The Strouhal number, St, relationship was used to determine the expected shedding frequency of the SPCCs. Based on the calculated Reynolds number range, the porous cylinders are expected to exhibit an approximate Strouhal number of 0.19 [14]; this value is used solely for estimating the shedding tone frequencies. The relationship between Strouhal number and the vortex shedding frequency is provided by $f = StU/D$, where f is the expected vortex shedding frequency (Hz) and U is the freestream speed of the water (m/s) and D is the outer diameter of the SPCC (m). Based on the values used in this study, the expected vortex shedding frequency range is from 0.6 Hz to 1.6 Hz. Such low shedding frequencies allow for the use of time-resolved PIV analysis that can capture a full vortex shedding cycle.

B. Structured porous coating designs

The porous structure of the coatings of each cylinder differ in their shape and subtly in their pore sizes. One design possesses elliptical-shaped pores, the other square-shaped pores. Photographs of these cylinders are presented in Fig. 2 to help illustrate the porous coating structure. The elliptical-shaped pore SPCC (shown in Fig. 2(a)) has identical proportions to the SPCC introduced in Arcondoulis et al. [7] that possesses an outer diameter of 60 mm. The SPCC is linearly scaled in the axial directions (not the spanwise directions) by a factor of 96 mm / 60 mm = 1.6 relative to the SPCC used in the previous study. The porous coating is comprised of three circular ring structures from the bare cylinder surface to the outer surface to produce four cylindrical layers, that can be observed in Fig. 2(a). In the vertical direction, the rings remain circular in structure (i.e., the cylindrical layers are equispaced in the radial direction). As the overall cylinder diameter increases with further distance from the cylinder center, the pores possess the same width in the spanwise direction as the lower layers, yet expand in the circumferential direction thus creating elliptical shaped pores (i.e., the difference between the long and short axes of the elliptical pores increases with radial distance from the center). By using circular and elliptical shapes, the porous coating is able to be successfully manufactured using 3-D printing (vertical square-shaped structures can cause issues with structural stability during 3-D printing processes). This cylinder design is 3-D printed in one-piece using a transparent ultraviolet curing epoxy resin.

To ensure that at least one of the SPCCs was sufficiently transparent for successful tomographic PIV tests, a second SPCC is designed that possesses square-shaped pores, as presented in Fig. 2(b). The structural design is similar to the elliptical-shaped porous coating in that it possesses three square pores from the inner to the outer surface. This design is

(a) (b)

Fig. 2 Images of the porous structured coating of the cylinders that possess (a) elliptical-shaped pores and (b) square-shaped pores.

simpler than the elliptical-shaped pore SPCC due to the lack of curved edges in the supporting members within the porous coating. The square-shaped pore SPCC was manufactured from a transparent acrylic using CNC machining. The material used for this cylinder design is more transparent than the elliptical-shaped pore SPCC. Furthermore, using square-shaped pores ensures that the structure that holds the cylindrical layers together has no curved edges. This improves the overall transparency of the model relative to the elliptical-pore design, as it decreases the amount of scattered light that is caused by the curved edges in the elliptical-shaped pore SPCC. Therefore, the overall transparency of the square-shaped pore SPCC is much greater than the elliptical-shaped pore SPCC.

C. Porosity and PPI estimations

The porosity values, ϕ (%), of the SPCCs are calculated using the following relationship

$$\phi = 100 \times \left(1 - \frac{V_{\text{SPCC}}}{V_{\text{SC}}}\right) \tag{1}$$

where V_{SPCC} is the volume of the porous coating and V_{SC} is the volume of a solid equivalent annulus, with inner diameter d and outer diameter D. The CAD programs used to design each model can simply provide V_{SPCC}. The elliptical-shaped pore SPCC porosity is calculated to be 87 % and the square-shaped pore SPCC porosity as 81 %.

The PPI calculation of each of the coatings is more complicated and requires some approximations. The PPI is calculated in each dimension (circumferential, spanwise and radial) and is averaged in each direction to provide an overall PPI estimate. Both porous coating designs possess forty-two pores along their circumference and thus possess the same PPI value from a circumferential perspective. There exist four equispaced cylindrical layers from the bare cylinder surface to the outer cylinder surface (due to the existence of three pores in the radial direction). On each of the cylindrical layers, there exist 42-pores and thus the PPI for each layer will be different, due to the different diameters of each layer, yet they will be the same for both cylinder designs. The mean circumferential PPI is calculated to be 4.34, by knowing that each layer is equispaced between d = 64 mm to D = 96 mm. In the spanwise direction, the models differ. The elliptical-shaped pore SPCC has a pore every 5.5 mm (thus 4.62 PPI) and the square-shaped pore SPCC has a pore every 8 mm (thus 3.18 PPI). The radial PPI is the same for both models, being the distance between the cylindrical layers (4 mm) and is thus 6.35 PPI. Therefore, the elliptical-shaped and square-shaped pore SPCC have overall values of 5.1 PPI and 4.6 PPI, respectively. Table 1 provides a summary of the SPCC parameters.

Table 1 Summary of the SPCC parameters.

SPCC	t (mm)	d (mm)	D (mm)	t/d	L (mm)	PPI	ϕ (%)
Elliptical-shaped pores	16	64	96	0.25	385	5.1	87
Square-shaped pores	16	64	96	0.25	385	4.6	81

III. Experimental Methods

Water tunnel PIV experiments were conducted in the Department of Civil Engineering and Geosciences at The Delft University of Technology (TUDelft), The Netherlands. Two PIV methods were used in this study: tomographic and 2-D planar. Both single-frame and double-frame modes are used in this study. Tomographic PIV was used to record both the internal and external flow field of the porous coated cylinders and 2-D planar PIV was used to measure a larger region of the external flow field.

A. Water tunnel facility

The low-speed water tunnel has a working section of 400 mm wide and an open channel height of 500 mm. Note that the maximum water tunnel height should not be reached due to safety purposes. In these experiments, the maximum working height is approximately 300 mm. The tunnel is inclined at 5° and is driven by a pressure-pump. By increasing the flow pressure and observing the increasing water tunnel height, it was deemed that the flow speed should not exceed 1 m/s for safety purposes. Based on the expected vortex shedding frequencies of the SPCCs (see Section II A) and the capability of the water tunnel facility, two flow speeds are chosen, being U_1 = 0.1 m/s and and U_2 = 0.8 m/s. These two speeds ensure that time-resolved PIV could be obtained at a lower flow speed and a Reynolds number closer to other published data could be obtained at a higher flow speed (see Section II A), while maintaining safety in the laboratory.

B. PIV parameters

The water is seeded with fine silt particles of approximate mean diameter of 100 μm. Illumination is provided by a Quantel EverGreen200 Double-Pulse Nd:YAG laser (532 nm wavelength, 200 mJ per pulse). One spherical and two-to-three cylindrical lenses are aligned and placed to produce a 20 mm thick laser sheet for the tomographic PIV tests and a 1 mm thick laser sheet for the 2-D PIV tests. Near the water tunnel glass walls, LaVision Imagers LX 16M (16MPx, 7.4 μm pixel pitch) are placed with Nikon Micro-Nikkor prime lenses (60 mm for 2-D planar tests, 105 mm for tomographic tests). For the tomographic tests, Scheimpflug adapters are used to align the focal plane with the laser sheet (i.e., perpendicular to the water tunnel glass walls). Synchronization of the laser pulses and image acquisition is accomplished using a LaVision Programmable Timing Unit in combination with the LaVision DaVis 8 software package. In single-frame mode, sequences are obtained in 1000 image pairs, over a time duration of 66.7 s, with an acquisition frequency for image pairs of 15 kHz. In double-frame mode, sequences are also obtained in 1000 image pairs over a time duration of 66.7 s, with an acquisition frequency for image pairs of 15 kHz. The pulse separation between laser signals is 600 μs, corresponding to a particle displacement of 40 mm (28 px in the image plane) with a freestream speed of U_2 = 0.8 m/s. Table 2 summarizes the parameters used during the PIV experiments in this study. For clarity and identification purposes, the tests are labeled Tests 1, 2 and 3.

Table 2 Summary of PIV parameters.

Parameter	Set-up 1	Set-up 2	Set-up 3
Freestream speed (U) (& Re)	0.1 m/s (0.9×10^4)	0.1 m/s (0.9×10^4)	0.8 m/s (7.3×10^4)
PIV method	2-D	Tomographic	Tomographic
Frame type	Single-Frame	Single-Frame	Double-Frame
Lens focal length	60 mm	105 mm	105 mm
Focal ratio (f/#)	4	16	16
Field of view (FOV)	various	$40 \times 40 \times 20$ mm^3	$40 \times 40 \times 20$ mm^3
Acquisition frequency (f_{aq})	15 Hz	15 Hz	15 Hz
Pulse separation (Δt)	-	-	600 μs
Measurement time (T)	66.7 s	66.7 s	66.7 s
Number of samples (N)	1000	1000	1000
No. images for time-averaging	300	500	500

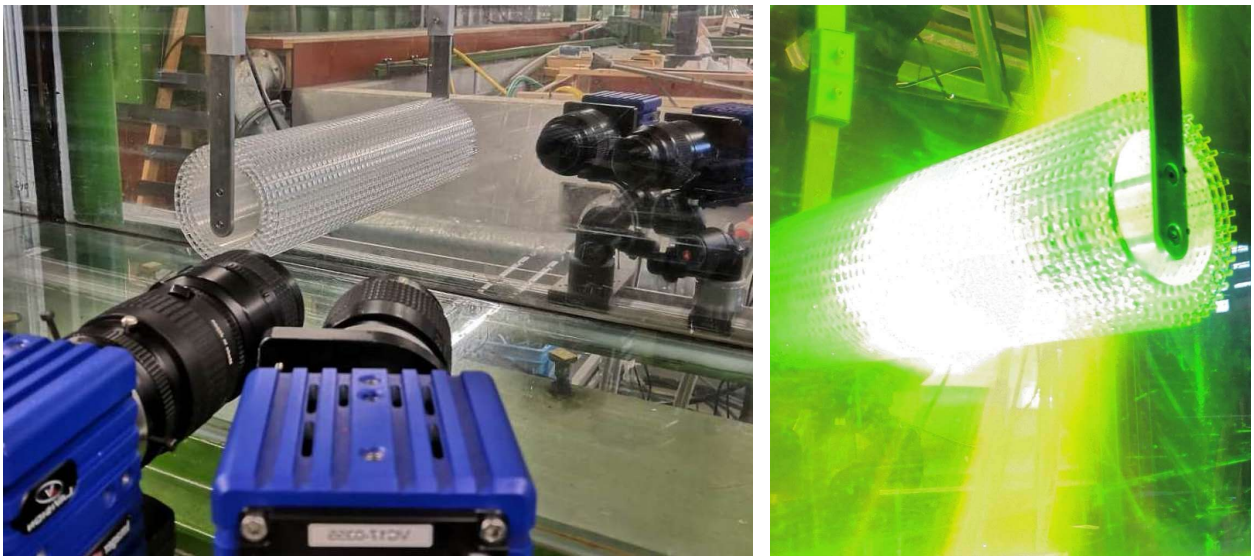

(a) (b)

Fig. 3 (a) Photo of the tomographic PIV set-up, showing the cameras aligned toward the square-shaped pore SPCC, corresponding to the camera angles in Fig. 4, (b) Laser light illuminating the rear of the square-shaped pore SPCC and the near-wake for tomographic PIV as depicted in Fig. 4.

C. PIV set-up

1. Tomographic PIV

Tomographic PIV set-up schematic diagrams of the side and top views are presented in Fig. 4. The mirror that reflects the laser sheet into the water is oriented such that a portion of the porous coated media and the cylinder wake are illuminated, as shown in Figs. 4(a) and 3(b). The tomographic FOV encompasses a 40 mm × 40 mm × 20 mm volume, that incorporates the porous coating at the rear of the cylinder and some of the wake region. Four-cameras are aligned toward the spanwise centerline of the SPCCs to obtain tomographic PIV images as depicted in Fig. 4(b) and shown in 3(a).

To conduct the calibration for the tomographic PIV tests (Set-up 2 & 3), a Type-7 calibration plate is placed in contact with the cylinder surface, to represent a portion of the FOV. The tunnel is filled with water (at zero velocity) to ensure that any refraction effects between water and air were factored into the calibration (as compared to leaving the calibration plate in air, with an empty water tunnel). Images are acquired with a calibration plate placed at three spanwise planes with the same the same xy-coordinates ; in the spanwise-center of the laser sheet and at the laser sheet edges (i.e., z = -10 mm, 0 mm and 10 mm). Using these images, the LaVision DaVis 8 software package is used to complete the calibration stages.

2. 2-D planar PIV

The 2-D planar PIV set-up schematic diagrams of the side and top views are presented in Fig. 5. A series of cylindrical lenses and the mirror are adjusted such that a large but thin laser sheet illuminates the entire cylinder diameter and some of the leeward and windward regions. The 2-D PIV is conducted with two cameras facing the same direction (in-parallel) to double the FOV. One camera is faced toward the front of the cylinder, the other toward the rear. Two FOVs are used with 120 mm × 120 mm areas that possess a 5 mm overlap, yet due to the limitations of the size of the laser sheet, not all of the FOV is not illuminated. During post-processing, geometric masking is applied to remove areas (corner regions) that are not illuminated. The 2-D planar calibration for Set-up 1 is simply conducted using 1 mm sheet paper in the plane of the laser sheet.

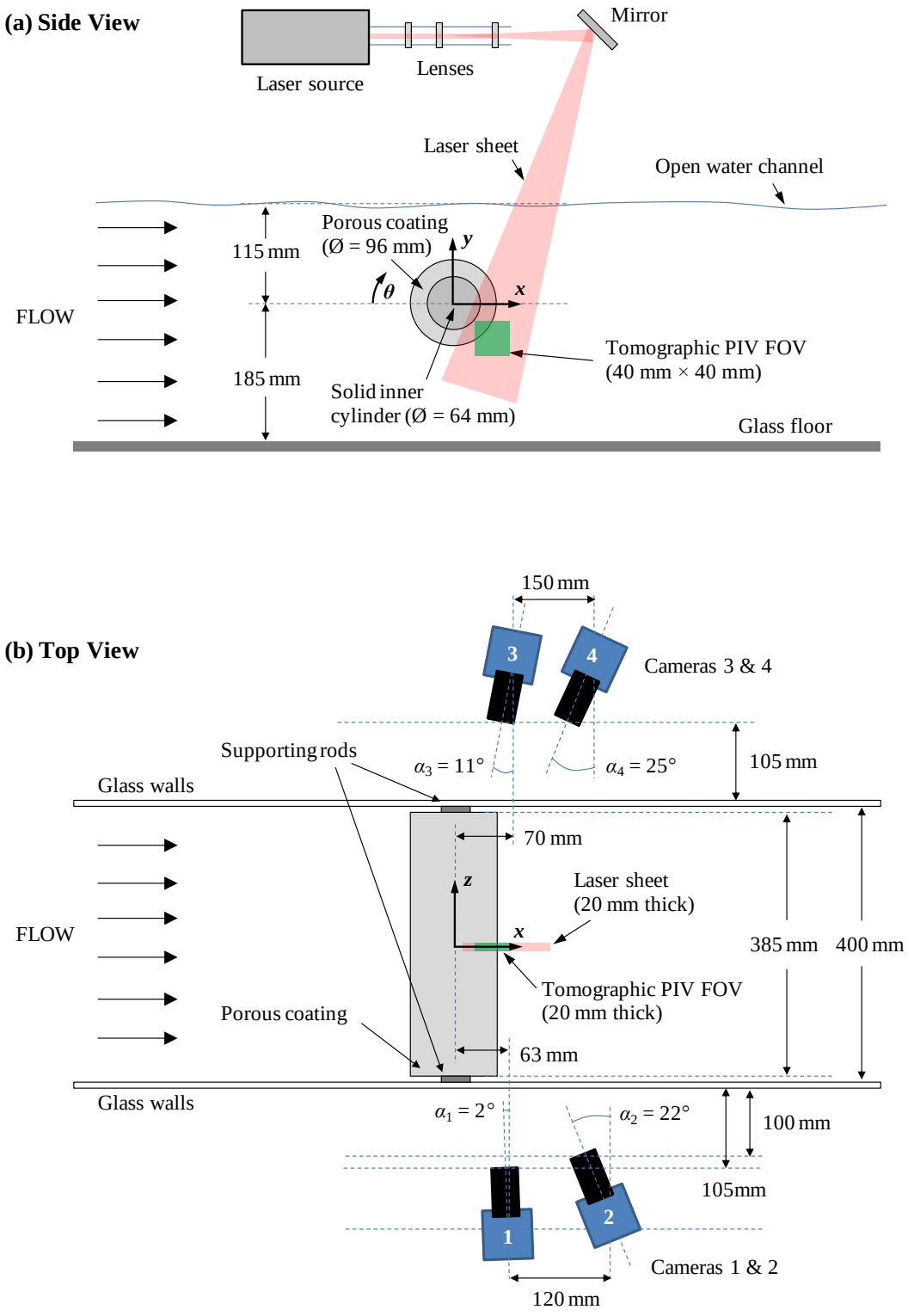

Fig. 4 Schematic diagram of the tomographic PIV configuration (Set-up 2 & 3) (a) Side view and (b) Top View.

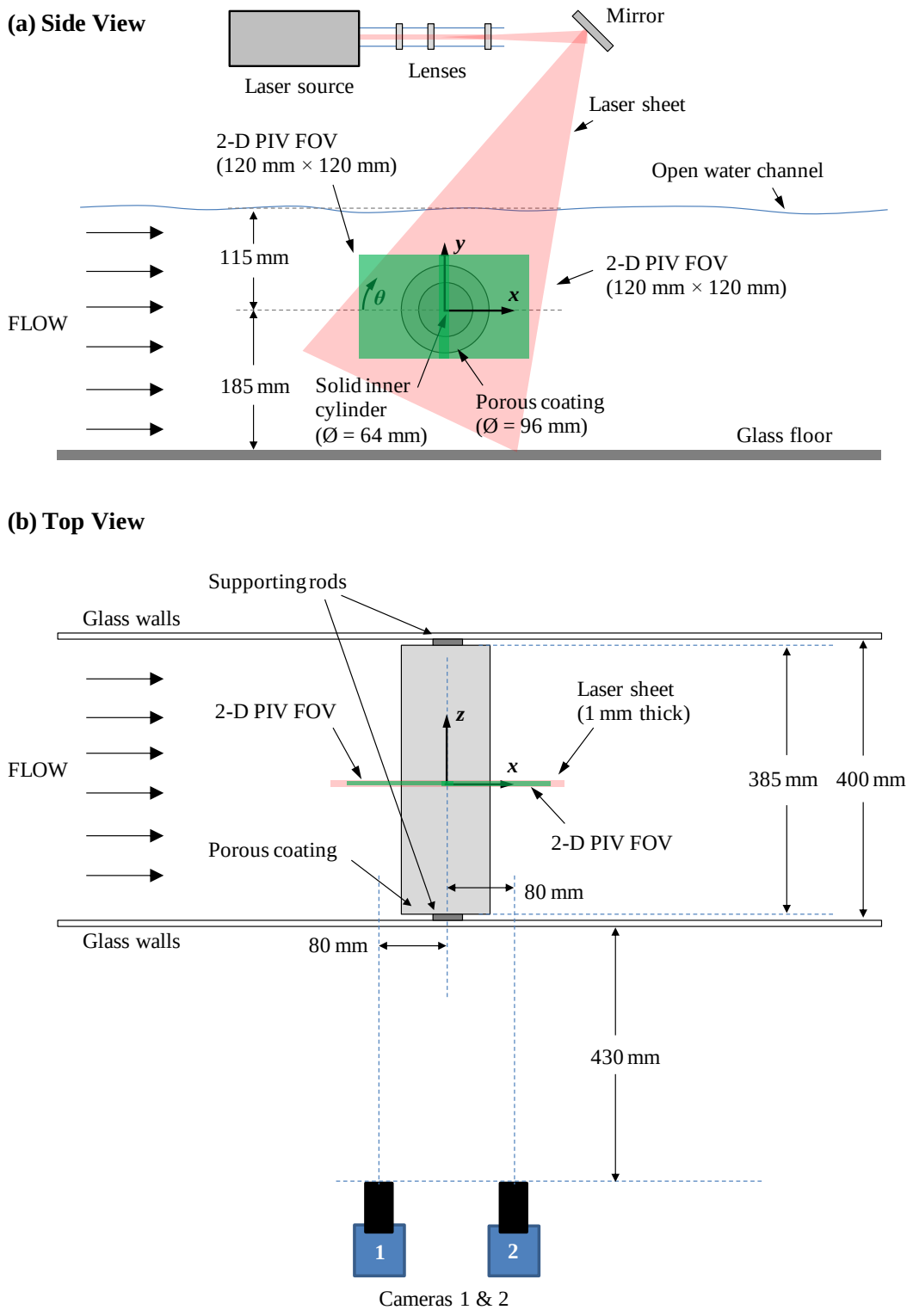

Fig. 5 Schematic diagram of the 2-D planar PIV configuration (Set-up 1) (a) Side view and (b) Top View.

IV. Results

A. 2-D Planar PIV

The near-wakes of the two SPCCs are investigated, to determine the differences in external flow fields and how the flow exits the porous structure. Figure 6 presents the x-component of velocity (U_x) for both cylinders, with a freestream velocity of U_1 = 0.1 m/s. Two structural members and the pore created by them are identified in Fig. 6 to help visualize the porous coating structures. Each of the tests were conducted using Set-up 1, as listed in Table 2.

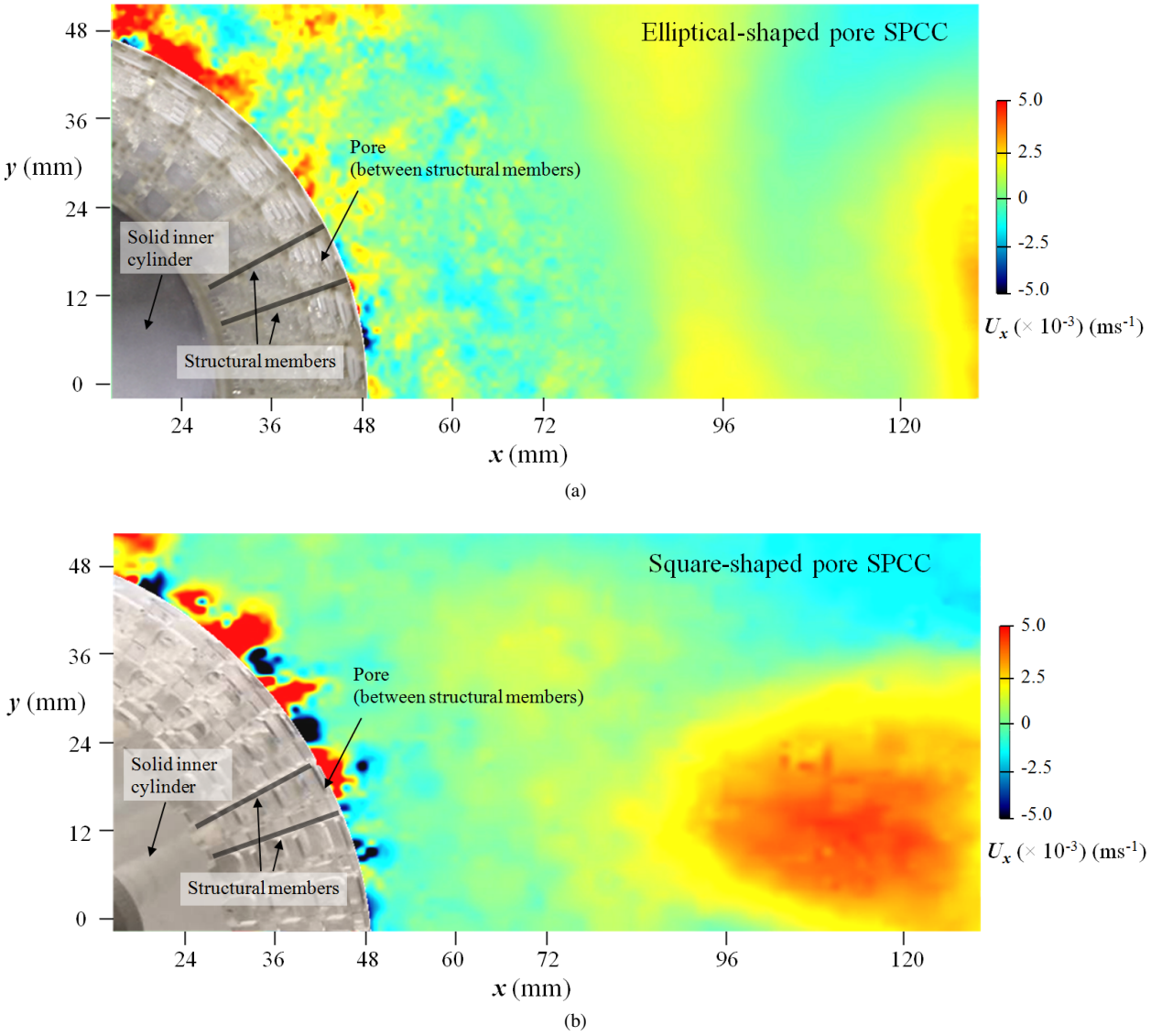

Fig. 6 2-D Planar PIV results, revealing the time-averaged values of U_x of the leeward surfaces of (a) Elliptical-shaped pore SPCC and (b) Square-shaped pore SPCC. Images are obtained in the cylinder spanwise mid-plane (z = 0 mm). Flow is from left to right with a freestream speed of U_1 = 0.1 m/s.

From Table 1, the elliptical-shaped pore SPCC has a porosity value that is 6% greater than the square-shaped porous coated structure. Also the structural members of the porous coating of the square-shaped SPCC are much thicker than the elliptical-shaped pore SPCC. Therefore, it is expected that the relatively small portion of fluid that exits the elliptical-shaped porous coating should pass through with less vorticity and reverse flow in the x-direction than the square-shaped porous coating. This can be observed by comparing Figs. 6(a) and 6(b), whereby at the cylinder leeward surface the flow patterns of U_x differ. This may be due to a recirculation of the flow, transitioning from internal to

external flow. Near the upper surface of the SPCC (positive y-direction), the elliptical-shaped pore SPCC possesses a much smaller reverse flow region than the square-shaped pore SPCC. Furthermore in the near wake of the square-shaped pore SPCC, an alternating pattern of negative-to-positive flow is observed, due to the rotational nature of the flow exiting the cylinder. Note that the spacing between these negative-to-positive flow regions corresponds closely to the spacing between the pores.

The flow on the windward-side is also investigated. Streamlines of the windward flow field for the elliptical-shaped pore SPCC are presented in Fig. 7. It can be observed as the flow travels from left to right that the freestream encounters the SPCC and the much of the flow passes around the cylinder, similar to the typical flow around a solid cylinder. Near the cylinder surface, some of the flow does not pass around the cylinder and enters instead. This can be observed within x = -48 mm to -14 mm and y = -10 mm to 50 mm. The streamlines appear to enter the porous coating and an accelerated flow region is also observed outside of this recirculating flow region. On the lower surface near y = -20 mm to -50 mm it can be inferred that some of the flow passes through the porous coating and exits toward x = -48 mm to -14 mm. These key features are labeled in Fig. 7.

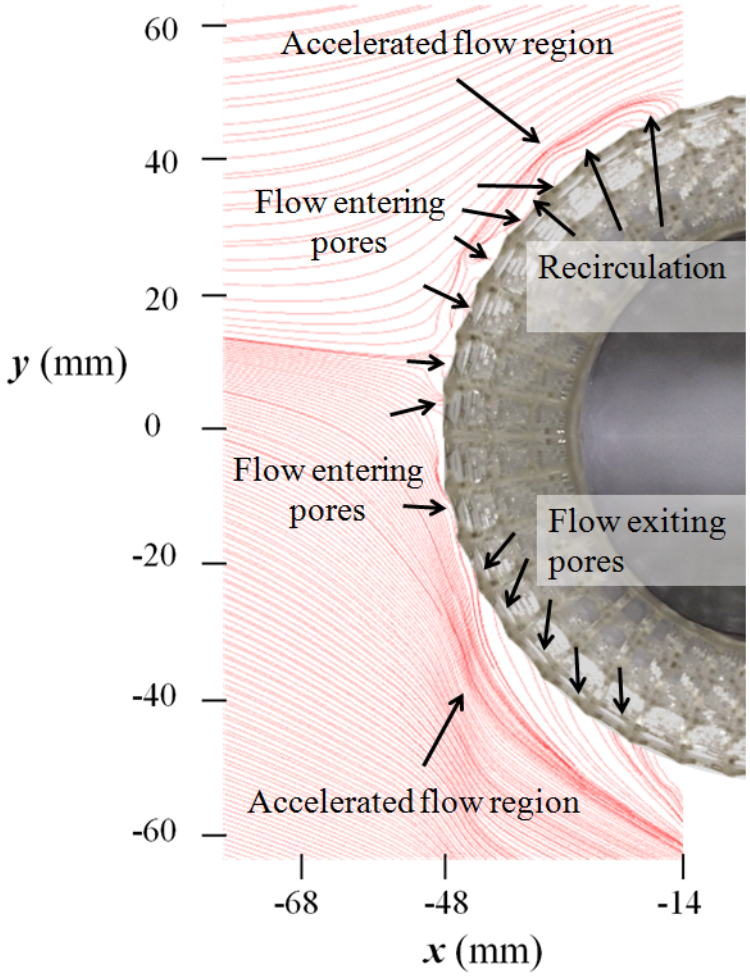

Fig. 7 2-D Planar PIV results, revealing the streamlines of the freestream flow interacting with the elliptical-shaped pore SPCC. Flow is from left to right with a freestream speed of U_1 = 0.1 m/s.

A portion of the elliptical-shaped pore SPCC span is investigated, by mounting the cylinder vertically and keeping the laser direction and all other parameters per Set-up 1, as listed in Table 2. The FOV plane is an xz-plane at y = 0 mm. The FOV is increased such that z = 120 mm of the cylinder span is observed. The image is cropped to a x = 40 mm × z = 120 mm window. Figure. 8 reveals the time-averaged vorticity about the y-axis (ω_y) along the cylinder span. As the flow approaches the cylinder windward side, the flow decreases in velocity at it approaches its stagnation point. However, due to the porous nature of the cylinder outer coating, some of the flow is capable of entering the

cylindrical structure and thus a vorticity-pattern is observed near the surface. From approximately z = -60 mm to 20 mm the alternating pattern of positive to negative vorticity is spaced similarly to the pore spacing. As the freestream flow approaches the porous coating, some of the particles in the flow have a clear path into the cylinder and some collide directly into the porous structural members. This causes a series of small stagnation points along the cylinder span and regions of accelerated and turbulent flow around the structural members. Flow particles that are to either side of these structural members will either enter the cylinder or travel around the cylinder in another path that involves some travel in the y-direction (out-of-plane motion that cannot be inferred from these planar data). The particles on one side of the structural members will follow a clockwise motion as the flow passes around the structural member and on the other side, a counter-clockwise fluid motion, thus revealing the alternating pattern of positive to negative vorticity. Therefore considering only the particles that remain in the current xz-plane, it can be inferred from the alternating positive and negative ω_y-values that the flow has indeed entered the porous coated medium and that the development of the flow around the cylinder is affected by the size of the pores and the PPI. From this preliminary result it can also be inferred that for improved passive control of the cylinder, a porous coated medium with varying porosity along the cylinder span (z-direction) could have significant impact on the development on the overall flow development around the cylinder by potentially impacting the spanwise coherence of the cylinder. It should be noted that at a Reynolds number of approximately $Re = 10^4$, the correlation length of a bare cylinder is approximately $5D$ [14]. The current investigation is conducted over 120 mm / 96 mm ≈ $1.2D$ (or ≈ $2d$) which is insufficient to make any conclusions regarding the spanwise coherence of a SPCC.

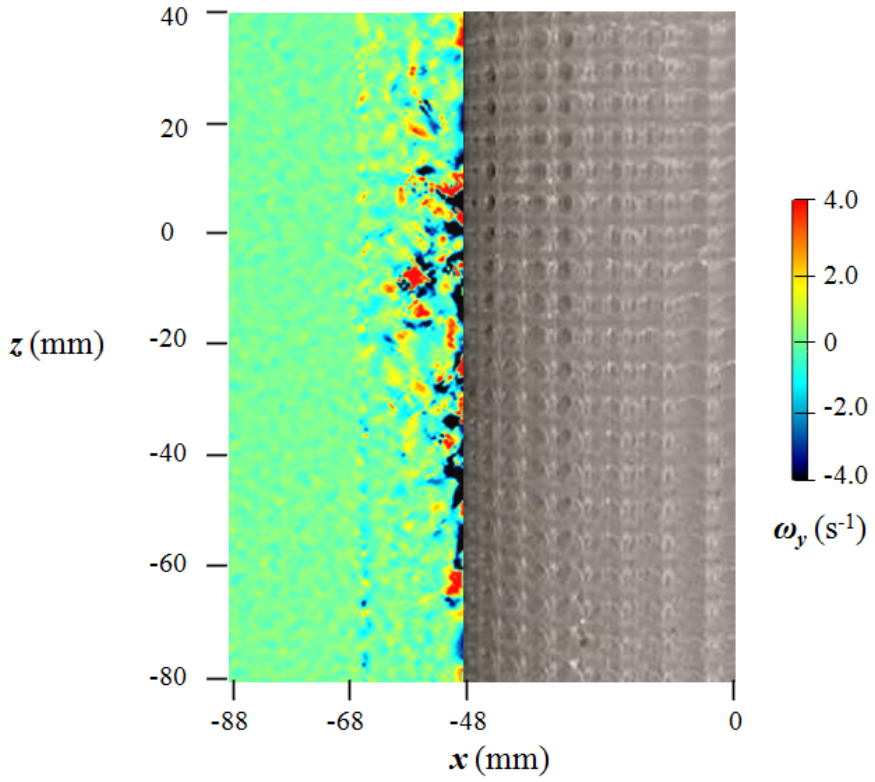

Fig. 8 2-D Planar PIV results, revealing the time-averaged values of ω_y of the windward surface of the elliptical-shaped pore SPCC along the span. Images are obtained along the cylinder center axis (y = 0 mm). Flow is from left to right with a freestream speed of U_1 = 0.1 m/s.

B. Tomographic PIV

Due to time constraints, the tomographic PIV results unfortunately are not presented in this paper. All of the data have been collected and will be processed and presented at a later date. During the experiments, the particles were clearly seen to enter and exit the porous coating for both cylinder designs via the live-mode of the DaVis 8 software. An example image, captured from Camera 2 (refer Fig. 4), reveals the illuminated particles both inside and outside of the square-shaped pore SPCC. Tomographic PIV tests were conducted using Set-up 2 & 3, for three separate FOVs. Figure. 4 depicts one of the FOVs; the others are placed at the windward area of the cylinder (i.e, the FOV is mirrored about the y-axis) and another at the bottom of the cylinder (i.e., its geometric center is the intersection of the cylinder's outer diameter and the y-axis). These data once processed will reveal some of the internal flow field characteristics of both SPCCs and help identify some of the porous coating key parameters by comparing the differences between the different cylinder flow fields.

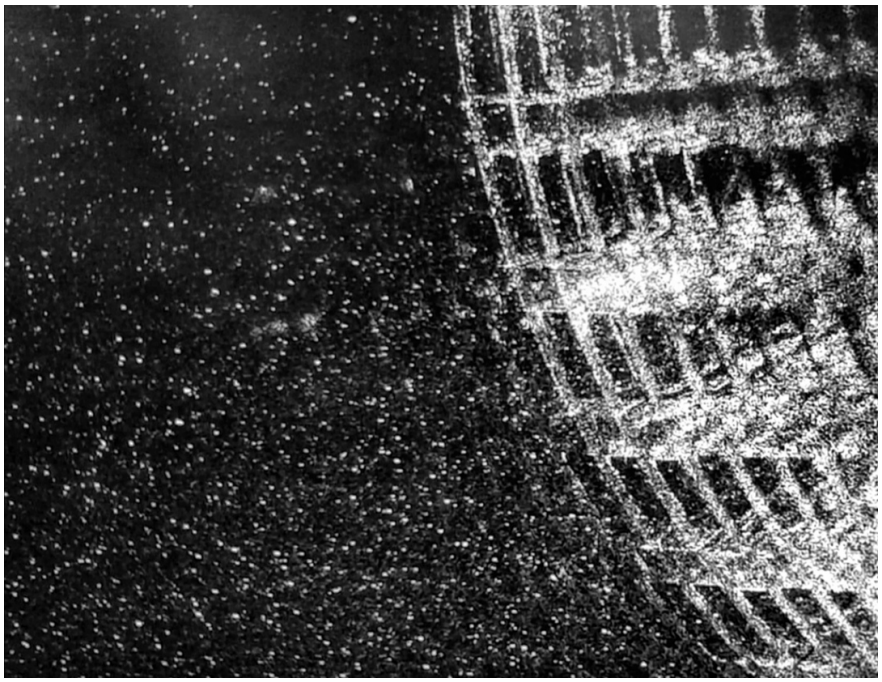

Fig. 9 Instantaneous snapshot from Camera 2 during a tomographic PIV test (using Set-up 2) revealing the illuminated particles both inside and outside of the square-shaped pore SPCC. Flow is from left to right with a freestream speed of U_1 = 0.1 m/s.

V. Conclusion

Two SPCCs have been designed and tested in a water tunnel using 2-D planar and tomographic PIV. To date, only the 2-D planar results have been processed. These results revealed some interesting differences in the near-wake flow region of both cylinders. It appears that at a Reynolds number of approximately 0.9×10^4 the square-shaped pore SPCC possesses greater recirculation through the rear of the porous structure than the elliptical-shaped pore SPCC. This is inferred by the alternating negative-to-positive flow region in the x-direction displayed by the square-shaped pore SPCC yet not by the elliptical-shaped pore SPCC. The two cylinders possess only small differences in porosity and PPI, yet from these preliminary results such small differences in porous properties may have significant influences on the internal and external flow fields. The flow along the spanwise direction reveals a similar alternating negative-to-positive region of out-of-plane vorticity near the windward surface of the elliptical-shaped pore SPCC. This may be explained by the flow entering the porous structure, colliding with a structural member and causing clockwise and counter-clockwise rotation around the member and hence alternating negative-to-positive vorticity along the span. These 2-D planar PIV results show that by making subtle changes to the porous structure that the flow in the near-wake can be modified. Previous studies have shown that influencing the wake of a cylinder has implications on the strength of vortex shedding

tones and therefore by careful manipulation of the structured porous coating, improved porous coatings can be designed for greater passive control of vortex shedding tones produced by cylinders in freestream flows.

As little is known about the effectiveness and mechanisms by which porous coated media act as a form of passive noise control, there is much work to be done and the authors are undertaking an ongoing investigation. During these water tunnel experiments a significant amount of data was collected using tomographic PIV at various locations along the cylinder circumference that was not presented in this paper due to time constraints. These data will require a large amount of time to post-process and analyze. Future work will include processing these data to determine the implications of using a porous coating on a cylindrical surface in the near wake, at a 90° radial location and at the front of the cylinder. By testing cylinders with much longer spans and smaller diameters (such that $L/D \approx 6$) in a wind tunnel, two hot-wire anemometry probes will be used simultaneously to determine the spanwise coherence length of SPCCs and randomized porous coatings, which will help identify key differences in the noise reduction mechanisms of structured porous coatings as compared to randomized porous coatings. Numerical analysis will include investigating the effect of porosity of an SPCC as a function of radial, circumferential and spanwise directions. This investigation may lead to aeroacoustically-optimized designs of porous coated cylinders for commercial and industrial applications. Furthermore, to totally visualize the internal flow field of a SPCC, an index refraction method could be used inside a suitable water tunnel. This would ensure that the cylinder would become totally transparent and thus relatively simple 2-D PIV can be used to visualize the internal flow field.

Acknowledgments

This research was supported by the National Natural Science Foundation of China (Grant No. 11772146) and the Aerodynamic Noise Control Laboratory of CARDC (Grant No. ANCL20180104). The authors would like to thank Sander de Vree (Department of Civil Engineering and Geosciences, TUDelft) for granting use of the water tunnel and his patience with our experimental procedures and requests, Victor Chavarrias for his assistance in organizing and booking the water tunnel facility and the workshop staff for their assistance and patience during testing. The primary author would also like to acknowledge Pengwei Xu (Research Assistant, Department of Mechanics and Aerospace Engineering, SUSTech), for his assistance in communicating with 3-D printing manufacturers and suppliers.

References

[1] Sueki, T., Ikeda, M., and Takaishi, T., "Aerodynamic noise reduction using porous materials and their application to high-speed pantographs," *Quarterly Report of RTRI*, Vol. 50, No. 1, 2009, pp. 26–31.

[2] Boorsma, K., Zhang, X., Molin, N., and Chow, L. C., "Bluff Body Noise Control Using Perforated Fairings," *AIAA Journal*, Vol. 47, No. 1, 2009, pp. 33–43.

[3] Liu, H., Wei, J., and Qu, Z., "Prediction of aerodynamic noise reduction by using open-cell metal foam," *Journal of Sound and Vibration*, Vol. 331, No. 7, 2012, pp. 1483–1497.

[4] Geyer, T. F., and Sarradj, E., "Circular cylinders with soft porous cover for flow noise reduction," *Experiments in Fluids*, Vol. 57, No. 3, 2016, p. 30.

[5] Geyer, T. F., Sharma, S., and Sarradj, E., "Detached Eddy Simulation of the Flow Noise Generation of Cylinders with Porous Cover," *Proceedings of the 2018 AIAA/CEAS Aeroacoustics Conference*, AIAA Paper 2018-3472 (2018).

[6] Klausmann, K., and Ruck, B., "Drag reduction of circular cylinders by porous coating on the leeward side," *Journal of Fluid Mechanics*, Vol. 813, 2017, pp. 382–411.

[7] Arcondoulis, E., Liu, Y., Li, Z., Yang, Y., Wang, Y., and Li, W., "The design and noise characteristics of a structured porous coated cylinder in uniform flow," *Proceedings of the 2018 AIAA/CEAS Aeroacoustics Conference*, AIAA Paper 2018-2963 (2018).

[8] Sueki, T., Takaishi, T., Ikeda, M., and Arai, N., "Application of porous material to reduce aerodynamic sound from bluff bodies," *Fluid dynamics research*, Vol. 42, No. 1, 2010, p. 015004.

[9] Aguiar, J., Yao, H., and Liu, Y., "Passive Flow/Noise Control of a Cylinder Using Metal Foam," *Proceedings of the 23rd International Congress on Sound and Vibration*, 2016, pp. 1–8.

[10] Ruck, B., Klausmann, K., and Wacker, T., "The flow around circular cylinders partially coated with porous media," *AIP Conference Proceedings*, Vol. 1453, No. 1, 2011, pp. 49–54.

[11] Zdravkovich, M., "Review and classification of various aerodynamic and hydrodynamic means for suppressing vortex shedding," *Journal of Wind Engineering and Industrial Aerodynamics*, Vol. 7, No. 2, 1981, pp. 145–189.

[12] Liu, H., and Azarpeyvand, M., "Passive Control of Tandem Cylinders Flow and Noise Using Porous Coating," *Proceedings of the 22nd AIAA/CEAS Aeroacoustics Conference*, AIAA Paper 2016-2905 (2016).

[13] Szepessy, S., "On the spanwise correlation of vortex shedding from a circular cylinder at high subcritical Reynolds number," *Physics of Fluids*, Vol. 6, No. 7, 1994, pp. 2406–2416.

[14] Norberg, C., "Fluctuating lift on a circular cylinder: review and new measurements," *Journal of Fluids and Structures*, Vol. 17, No. 1, 2003, pp. 57–96.

[15] Naito, H., and Fukagata, K., "Numerical simulation of flow around a circular cylinder having porous surface," *Physics of Fluids*, Vol. 24, No. 11, 2012.

[16] Bruneau, C.-H., and Mortazavi, I., "Numerical modelling and passive flow control using porous media," *Computers & Fluids*, Vol. 37, No. 5, 2008, pp. 488–498.

[17] Xu, C., Mao, Y., and Hu, Z., "Numerical study of pore-scale flow and noise of an open cell metal foam," *Aerospace Science and Technology*, Vol. 82, 2018, pp. 185–198.

[18] Yuana, H., Xiab, C., Chenc, Y., and Yangd, Z., "Flow around a finite circular cylinder coated with porous media," *Proceedings of the 8th International Colloquium on Bluff Body Aerodynamics and Applications*, 2016.

[19] Jenkins, L., Neuhart, D., McGinley, C., Khorrami, M., and Choudhari, M., "Measurements of unsteady wake interference between tandem cylinders," *Proceedings of the 36th AIAA Fluid Dynamics Conference and Exhibit*, 2006, p. 3202.

[20] Neuhart, D., Jenkins, L., Choudhari, M., and Khorrami, M., "Measurements of the flowfield interaction between tandem cylinders," *Proceedings of the 15th AIAA/CEAS Aeroacoustics Conference*, AIAA Paper 2009-3275 (2009).

[21] Hutcheson, F. V., Brooks, T. F., Lockard, D. P., Choudhari, M. M., and Stead, D. J., "Acoustics and Surface Pressure Measurements from Tandem Cylinder Configurations," *Proceedings of the 20th AIAA/CEAS Aeroacoustics Conference*, AIAA Paper 2014-2762 (2014).